



## Synthesis, spectroscopy and computational studies of some novel phosphorylated derivatives of quinoline-5,8-diones

Jacek E. Nycz<sup>a,\*</sup>, Grzegorz Malecki<sup>a</sup>, Lukasz Ponikiewski<sup>c</sup>, Markus Leboschka<sup>d</sup>, Maria Nowak<sup>b</sup>, Joachim Kusz<sup>b</sup>

<sup>a</sup> Institute of Chemistry, University of Silesia, ul. Szkolna 9, PL-40007 Katowice, Poland

<sup>b</sup> Institute of Physics, University of Silesia, ul. Uniwersytecka 4, PL-40007 Katowice, Poland

<sup>c</sup> Department of Inorganic Chemistry, Faculty of Chemistry, Gdańsk University of Technology, 11/12 G. Narutowicz St., PL-80233 Gdańsk, Poland

<sup>d</sup> Institut für Anorganische Chemie, Universität Stuttgart, Pfaffenwaldring 55, 70550 Stuttgart, Germany

### ARTICLE INFO

#### Article history:

Received 15 September 2010

Accepted 11 November 2010

Available online 25 November 2010

#### Keywords:

Quinoline

Quinone

Phosphorylation

Single-Electron Transfer (SET)

DFT

X-ray

### ABSTRACT

The neutral phosphorus nucleophiles such as  $R_2P(=Y)M$  [**1a–f**,  $Y=O$  or lone pair;  $R = Ph, tBu, OCH_2C(CH_3)_2CH_2O, Pr^iO, EtO$  or  $MeO$ ;  $M = H$  or  $SiMe_3$ ] allowed the radical addition to 2-methyl-5,8-dioxo-5,8-dihydroquinoline-7-amine (**2a**) and *N*-(2-methyl-5,8-dioxo-5,8-dihydroquinolin-7-yl)acetamide (**2b**) giving exclusively *O*-phosphorylated products, i.e.: 7-acetylamino-5-hydroxy-2-methylquinolin-8-yl diphenylphosphinate (**3a**), 7-acetylamino-5-hydroxy-2-methylquinolin-8-yl *t*-butylphenylphosphinate (**3b**), 7-acetylamino-5-hydroxy-2-methylquinolin-8-yl diisopropyl phosphate (**3c**), 7-acetylamino-5-hydroxy-2-methylquinolin-8-yl diethyl phosphate (**3d**), *N*-{8-[(5,5-dimethyl-2-oxido-1,3,2-dioxaphosphinan-2-yl)oxy]-5-hydroxy-2-methylquinolin-7-yl}acetamide (**3e**), 7-amino-5-hydroxy-2-methylquinolin-8-yl dimethyl phosphate (**3f**) and 7-amino-5-hydroxy-2-methylquinolin-8-yl *t*-butylphenylphosphinate (**3g**), respectively, with high yield. All products were quantitatively prepared and characterized by microanalysis, and multinuclear NMR spectroscopy. Seven of them, i.e.: **2a**, **2b**, **3a**, **3b**, **3d**, **3e** and **3g** have been characterized by single crystal X-ray diffraction method. The geometries of the studied compounds were optimized in singlet states using the density functional theory (DFT) method with B3LYP functional. The redox properties of **2a** and **2b** have been studied using cyclic voltammetry. The reduction corresponds to the electrochemical behaviour of naturally occurring quinones.

© 2010 Elsevier B.V. All rights reserved.

### 1. Introduction

The quinones are a class of compounds of great interest from the synthetic, theoretical and applications point of view [1–3]. Among them, the 1-(7-amino-5,8-dioxo-5,8-dihydroquinolin-2-yl)-4-methyl-9*H*- $\beta$ -carboline-3-carboxylic acid (shortly named lavendamyacin) has attracted special attention due to its broad spectrum antitumor, antibacterial and antiviral activity [4–7].

The redox properties of biologically important hydroquinone/*p*-quinone systems are well known [3]. Three quinones, viz., coenzyme Q (ubiquinone), plastoquinone and menaquinone are among the most important biological electron carriers. One-electron reduced forms, the semiquinone anion radicals, are directly involved in electron transfer reactions within photosynthesis and respiration. They are strongly affected by the surrounding medium, by pH and temperature, particularly if the corresponding electron

transfer reaction is part of an electron transport chain embedded in the mitochondrial inner membranes [8].

Phosphorus plays a crucial role in the biochemistry of all living beings. Incorporation of phosphorus containing groups into biologically active compounds or their structural analogues could be of interest for at least two important reasons. First,  $^{31}P$  NMR spectroscopy offers good opportunities to better understand the biological profile of potential activity, and it has been established as a useful, non-perturbing tool for probing effects at the phosphorus atoms. The NMR properties of the phosphorus-31 nucleus are well suited for in vivo NMR because of its natural abundance (100%), reasonable sensitivity, and adequate but not excessive chemical shifts. Changes in  $^{31}P$  chemical shifts can be helpful to understand several kinds of interactions such as hydrogen bonding or protonation, without introducing any modifications that could alter the structure. Secondly, some key metabolites, particularly those involved in the production of energy, contain phosphorus and are present in substantial concentrations in living tissues [9,10].

The biological activity of lavendamyacin may be connected with the presence of a quinoline-5,8-dione subunit. To the best of our

\* Corresponding author. Tel.: +48 323591206; fax: +48 322599978.

E-mail address: [jnycz@us.edu.pl](mailto:jnycz@us.edu.pl) (J.E. Nycz).

knowledge only few examples of phosphorylated derivatives of lavendomycin have been reported so far [11]. Surprisingly, there is no example of a phosphorylated quinoline-5,8-dione unit reported. In consideration of the present knowledge of the reactivity of quinoline-5,8-diones, it is conceivable that further explorations in this field may lead to new applications, not only in the area of introducing a phosphorus containing moiety.

## 2. Experimental

### 2.1. General

All experiments were carried out in an atmosphere of dry argon, using Schlenk techniques. Solvents were dried by usual methods (benzene and THF over benzophenone ketyl,  $\text{CHCl}_3$  and  $\text{CH}_2\text{Cl}_2$  over  $\text{P}_4\text{O}_{10}$ , hexane over sodium–potassium alloy), distilled and degassed. Chromatography was carried out on Silica Gel 60 (0.15–0.3 mm) Machery Nagel. NMR spectra were obtained with Bruker Avance 400 operating at 400.13 MHz ( $^1\text{H}$ ), 161.9 MHz ( $^{31}\text{P}$ ) and 100.4 MHz ( $^{13}\text{C}$ ) at 30 °C; chemical shifts referenced to ext. TMS ( $^1\text{H}$ ,  $^{13}\text{C}$ ), 85%  $\text{H}_3\text{PO}_4$  ( $\mathcal{E} = 40.480747$  MHz,  $^{31}\text{P}$ ); positive signs of chemical shifts denote shifts to lower frequencies, coupling constants are given as absolute values. Elemental analysis: Perkin–Elmer Analyzer 240. Mass spectra were obtained with a MASPEC II system [I132/99D9], Varian MAT 711 and Finnigan MAT 95 (Finnigan MAT GmbH, Bremen); in EI mode (70 eV) and, where necessary, LSI technique was applied. EPR spectra in the X-band were recorded with a Bruker System EMX. Cyclic voltammetry was carried out in 0.1 M  $\text{Bu}_4\text{NPF}_6$  solutions using a three-electrode configuration (glassy-carbon working electrode, Pt counter electrode, Ag wire as pseudoreference) and a PAR 273 potentiostat and function generator. The ferrocene/ferrocenium ( $\text{Fc}/\text{Fc}^+$ ) couple served as internal reference. Melting points were taken in sealed capillaries and are uncorrected. Compounds **2a**, **2b** [12] and **1a** [13] were synthesized according to procedures described in the literature. Reagents **1d** and **1f** were purchased from Aldrich, and **1c** from Acros Organics and were distilled before used.

### 2.2. X-ray crystallographic studies

Data for compounds **2a**, **2b** and **3a**, **3b**, **3d** were collected on a KUMA KM4 diffractometer with graphite-monochromated Mo  $K\alpha$  radiation using Sapphire-2 CCD detector. The apparatus was equipped with an open flow thermostat (Oxford Cryosystems) with enabled experiments at 120 K. The stream of nitrogen also prevented the specimen from contact with moisture and oxygen. The structure were solved by direct methods and refined by full-matrix least-squares on  $F^2$  (all data) using the SHELXTL program package [14]. All non-hydrogen atoms were refined anisotropically. Hydrogen atoms were refined in geometrically idealised positions with isotropic temperature factors 1.2 times the equivalent isotropic temperature factors Ueq of their attached atoms (1.5 for  $\text{CH}_3$  groups).

For compounds **3b** and **3e** the X-ray measurements were performed with Oxford Diffraction Xcalibur diffractometer equipped with a Sapphire3 CCD detector and graphite-monochromated Mo  $K\alpha$  radiation ( $\lambda = 0.71073$  Å). The crystal was cooled down to 100 K by a cold dry nitrogen gas stream (Oxford Cryosystems equipment). The temperature stability of the measurement was  $\pm 1$  K. During the data collection  $\omega$  scans were performed. No absorption corrections were used. The structure was first solved using the direct method with SHELXS-97 software [15] and then the solution was refined with SHELXL-97 [16]. All non-hydrogen atoms were refined with anisotropic temperature factors. All H atoms bound to C atoms were refined using a riding model with

C–H distances of 0.95 Å or 0.98 Å and Uiso(H) values of 1.2Ueq(C), or 1.5Ueq(C), respectively. H atoms, which take part in hydrogen bond, were permitted to ride at the positions deduced from the difference maps with Uiso(H) equal to 1.2Ueq(C), 1.2Ueq(N) or 1.5Ueq(O).

For compound **3g** the X-ray measurements were performed with Oxford Diffraction Xcalibur Gemini A diffractometer with graphite-monochromated Mo  $K\alpha$  radiation ( $\lambda = 0.71073$  Å). The crystal was measured at 265 K. During the data collection  $\omega$  scans were performed and absorption corrections were used. The structure was first solved using the direct method with SHELXS-97 software [15] and then the solution was refined with SHELXL-97 [16]. All non-hydrogen atoms were refined with anisotropic temperature factors. All H atoms bound to C atoms were refined using a riding model with C–H distances of 0.95 Å or 0.98 Å and Uiso(H) values of 1.2Ueq(C), or 1.5Ueq(C), respectively. H atoms, which take part in hydrogen bonds, were permitted to ride at the positions deduced from the difference maps with Uiso(H) equal to 1.2Ueq(C), 1.2Ueq(N) or 1.5Ueq(O).

### 2.3. Synthesis of **3a**, **3b** and **3g**

**2b** (5 mmol) in THF (100 mL) was added to the solution of **1a** or **1b** (5 mmol), respectively, in THF (25 mL) at room temperature. After complete addition the reaction mixture was heated at 60 °C for 16 h. Next, a sample of the reaction mixture was taken, DMSO-*d*<sub>6</sub> was added, and the  $^{31}\text{P}\{^1\text{H}\}$  NMR spectrum was recorded. Subsequently dry air was passed through the reaction mixture at room temperature, for **1a**. The volatiles were evaporated and the residue was purified by chromatography and crystallisation:

**3a** ( $\text{CH}_2\text{Cl}_2$ :MeOH = 5:1) 0.259 g (0.6 mmol, 12%); mp = 220–221 °C (MeOH);  $^1\text{H}$  NMR (400.13 MHz, DMSO-*d*<sub>6</sub>, 30 °C)  $\delta$  = 2.11 (s, 3H,  $\text{CH}_3$ ), 2.64 (s, 3H,  $\text{CH}_3$ ), 7.23 (d,  $J_{\text{H,H}} = 8.5$  Hz, 1H, quin-H), 7.42 (ddt,  $J_{\text{P,H}} = 7.3$  Hz,  $J_{\text{H,H}} = 3.7$  Hz,  $J_{\text{H,H}} = 1.2$  Hz, 4H, *m*-arom-H), 7.49 (ddd,  $J_{\text{P,H}} = 12.5$  Hz,  $J_{\text{H,H}} = 6.9$  Hz,  $J_{\text{H,H}} = 1.5$  Hz, 2H, *p*-arom-H), 7.57 (s, 1H, quin-H), 8.10 (dd,  $J_{\text{P,H}} = 12.5$  Hz,  $J_{\text{H,H}} = 7.1$  Hz, 4H, *o*-arom-H), 8.12 (d,  $J_{\text{H,H}} = 8.5$  Hz, 1H, quin-H), 9.80 (s, 1H, OH), 10.49 (s, 1H, NH);  $^{13}\text{C}\{^1\text{H}\}$  NMR (100.4 MHz, DMSO-*d*<sub>6</sub>, 30 °C)  $\delta$  = 24.59, 25.16, 103.00, 115.45, 120.29, 128.69 (d,  $J_{\text{P,C}} = 13.3$  Hz, P–Ph), 129.73, 131.08, 131.12, 131.23 (d,  $J_{\text{P,C}} = 3.4$  Hz, P–Ph), 132.36 (d,  $J_{\text{P,C}} = 10.6$  Hz, P–Ph), 133.16 (d,  $J_{\text{P,C}} = 2.8$  Hz, P–Ph), 150.25 (d,  $J_{\text{P,C}} = 1.5$  Hz), 159.27, 168.69;  $^{31}\text{P}\{^1\text{H}\}$  NMR (161.9 MHz, DMSO-*d*<sub>6</sub>, 30 °C)  $\delta$  = 36.28; MS: (LSI) ( $\text{M}+\text{H}$ )<sup>+</sup> 433; HRMS: *m/z* Calcd for  $\text{C}_{24}\text{H}_{22}\text{N}_2\text{O}_4\text{P}$  ( $\text{M}+\text{H}$ )<sup>+</sup>: 433.13176 Found 433.13172; E.A. [Found C, 64.67%; H, 5.50%; N, 6.03%;  $\text{C}_{24}\text{H}_{21}\text{N}_2\text{O}_4\text{P} \cdot \text{CH}_3\text{OH}$  requires C, 64.65%; H, 5.43%; N, 6.03%].

**3b** ( $\text{CH}_2\text{Cl}_2$ :MeOH = 5:1) 1.112 g (2.7 mmol, 54%); mp = 265–266 °C (MeOH);  $^1\text{H}$  NMR (400.13 MHz, DMSO-*d*<sub>6</sub>, 30 °C)  $\delta$  = 1.30 (d,  $J_{\text{P,H}} = 16.3$  Hz, 9H, *t*Bu), 2.09 (s, 3H,  $\text{CH}_3$ ), 2.64 (s, 3H,  $\text{CH}_3$ ), 7.30 (d,  $J_{\text{H,H}} = 8.5$  Hz, 1H, quin-H), 7.43 (dt,  $J_{\text{P,H}} = 7.6$  Hz,  $J_{\text{H,H}} = 3.5$  Hz, 2H, *m*-arom-H), 7.54 (dt,  $J_{\text{P,H}} = 6.7$  Hz,  $J_{\text{H,H}} = 1.1$  Hz, 1H, *p*-arom-H), 7.62 (s, 1H, quin-H), 8.08 (m, 2H, *o*-arom-H), 8.25 (d,  $J_{\text{H,H}} = 8.5$  Hz, 1H, quin-H), 10.43 (s, 1H, OH), 10.53 (s, 1H, NH);  $^{13}\text{C}\{^1\text{H}\}$  NMR (100.4 MHz, DMSO-*d*<sub>6</sub>, 30 °C)  $\delta$  = 23.91, 24.04, 24.70, 33.34 (d,  $J_{\text{P,C}} = 98.0$  Hz, P-*t*Bu), 102.84, 115.17, 119.89, 125.77, 126.92, 127.85 (d,  $J_{\text{P,C}} = 12.0$  Hz, P–Ph), 130.04 (d,  $J_{\text{P,C}} = 3.0$  Hz, P–Ph), 130.74, 132.72 (d,  $J_{\text{P,C}} = 2.0$  Hz, P–Ph), 133.27 (d,  $J_{\text{P,C}} = 9.7$  Hz, P–Ph), 140.70 (d,  $J_{\text{P,C}} = 3.2$  Hz), 149.48, 158.71, 168.03;  $^{31}\text{P}\{^1\text{H}\}$  NMR (161.9 MHz, DMSO-*d*<sub>6</sub>, 30 °C)  $\delta$  = 56.10; MS: (LSI) ( $\text{M}+\text{H}$ )<sup>+</sup> 413; HRMS: *m/z* Calcd for  $\text{C}_{22}\text{H}_{26}\text{N}_2\text{O}_4\text{P}$  ( $\text{M}+\text{H}$ )<sup>+</sup>: 413.16302 Found 413.16343; E.A. [Found C, 63.97%; H, 6.12%; N, 6.78%;  $\text{C}_{22}\text{H}_{25}\text{N}_2\text{O}_4\text{P}$  requires C, 64.07%; H, 6.11%; N, 6.79%].

**3g** (MeOH) 1.166 g (3.15 mmol, 63%); mp = 252 °C (MeOH);  $^1\text{H}$  NMR (400.13 MHz, DMSO-*d*<sub>6</sub>, 30 °C)  $\delta$  = 1.31 (d,  $J_{\text{P,H}} = 16.9$  Hz, 9H, *t*Bu), 2.78 (s, 3H,  $\text{CH}_3$ ), 6.71 (s, 1H, quin-H), 7.27 (d,  $J_{\text{H,H}} = 8.2$  Hz,

1H, quin-H), 7.55 (dt,  $J_{P,H} = 3.4$  Hz,  $J_{H,H} = 7.6$  Hz, 2H, P-Ph), 7.66 (t,  $J_{H,H} = 7.2$  Hz, 1H, *m*-Ph), 7.92 (m, 2H, *o*-Ph), 8.62 (bs, 1H, quin-H), 11.42 (s, 1H, OH), 14.82 (s, 1H, NH);  $^{13}\text{C}\{^1\text{H}\}$  NMR (100.4 MHz, DMSO-*d*<sub>6</sub>, 30 °C)  $\delta = 20.54, 23.86, 33.13$  (d,  $J_{P,C} = 95.7$  Hz, P-*t*Bu), 100.87, 113.15, 115.20, 116.90, 123.53, 124.62, 128.69 (d,  $J_{P,C} = 12.0$  Hz, P-Ph), 132.69 (d,  $J_{P,C} = 9.9$  Hz, P-Ph), 133.70, 139.57, 147.36, 152.27, 154.71;  $^{31}\text{P}\{^1\text{H}\}$  NMR (161.9 MHz, DMSO-*d*<sub>6</sub>, 30 °C)  $\delta = 62.96$ ; MS: (LSI) (M+H)<sup>+</sup> 371; HRMS: *m/z* Calcd for C<sub>20</sub>H<sub>24</sub>N<sub>2</sub>O<sub>3</sub>P (M+H)<sup>+</sup>: 371.16302 Found 371.16343; E.A. [Found C, 64.56; H, 6.11; N, 7.79; C<sub>20</sub>H<sub>23</sub>N<sub>2</sub>O<sub>3</sub>P requires C, 64.86%; H, 6.26%; N, 7.56%].

#### 2.4. Synthesis of 3c, 3d, 3e and 3f

**2a** or **2b** (5 mmol) in THF (100 mL) was added to the solution of **1c**, **1d**, **1e** or **1f** (20 mmol), respectively, in THF (25 mL) at room temperature. After complete addition the reaction mixture was heated under reflux for 16 h. Next, a sample of the reaction mixture was taken, DMSO-*d*<sub>6</sub> was added, and the  $^{31}\text{P}\{^1\text{H}\}$  NMR spectrum was recorded. The volatiles were evaporated and the residue was purified by chromatography and crystallisation:

**3c** (MeOH) 1.287 g (3.25 mmol, 65%); mp = 183 °C (MeOH);  $^1\text{H}$  NMR (400.13 MHz, DMSO-*d*<sub>6</sub>, 30 °C)  $\delta = 1.19$  (d,  $J_{H,H} = 6.1$  Hz, 6H, 2CH<sub>3</sub>), 1.30 (d,  $J_{H,H} = 6.1$  Hz, 6H, 2CH<sub>3</sub>), 2.12 (s, 3H, CH<sub>3</sub>), 2.62 (s, 3H, CH<sub>3</sub>), 4.99 (m, 2H, 2CH), 7.31 (d,  $J_{H,H} = 8.5$  Hz, 1H, quin-H), 7.59 (s, 1H, quin-H), 8.31 (d,  $J_{H,H} = 8.5$  Hz, 1H, quin-H), 9.42 (s, 1H, OH), 10.47 (s, 1H, NH);  $^{13}\text{C}\{^1\text{H}\}$  NMR (100.4 MHz, DMSO-*d*<sub>6</sub>, 30 °C)  $\delta = 23.06$  (d,  $J_{P,C} = 5.6$  Hz), 23.28 (d,  $J_{P,C} = 4.6$  Hz), 24.01, 24.63, 72.91 (d,  $J_{P,C} = 6.2$  Hz), 103.02, 115.24, 119.24, 127.72 (d,  $J_{P,C} = 8.7$  Hz), 130.38 (d,  $J_{P,C} = 4.0$  Hz), 130.66, 140.96 (d,  $J_{P,C} = 3.1$  Hz), 149.72 (d,  $J_{P,C} = 1.9$  Hz), 158.84, 168.12;  $^{31}\text{P}\{^1\text{H}\}$  NMR (161.9 MHz, DMSO-*d*<sub>6</sub>, 30 °C)  $\delta = -5.90$ ; MS: (LSI) (M+H)<sup>+</sup> 397; HRMS: *m/z* Calcd for C<sub>18</sub>H<sub>26</sub>N<sub>2</sub>O<sub>6</sub>P (M+H)<sup>+</sup>: 397.15194 Found 397.15211; E.A. [Found C, 54.50; H, 6.37; N, 7.05; C<sub>18</sub>H<sub>25</sub>N<sub>2</sub>O<sub>6</sub>P requires C, 54.54%; H, 6.36%; N, 7.07%].

**3d** (MeOH) 1.049 g (2.85 mmol, 57%); mp = 216 °C (MeOH);  $^1\text{H}$  NMR (400.13 MHz, DMSO-*d*<sub>6</sub>, 30 °C)  $\delta = 1.26$  (t,  $J_{H,H} = 7.0$  Hz, 6H,

2CH<sub>3</sub>), 2.12 (s, 3H, CH<sub>3</sub>), 2.62 (s, 3H, CH<sub>3</sub>), 4.36 (m, 4H, 2CH<sub>2</sub>), 7.31 (d,  $J_{H,H} = 8.5$  Hz, 1H, quin-H), 7.49 (s, 1H, quin-H), 8.32 (d,  $J_{H,H} = 8.5$  Hz, 1H, quin-H), 9.51 (s, 1H, OH), 10.49 (s, 1H, NH);  $^{13}\text{C}\{^1\text{H}\}$  NMR (100.4 MHz, DMSO-*d*<sub>6</sub>, 30 °C)  $\delta = 15.81$  (d,  $J_{P,C} = 6.9$  Hz), 23.74, 24.66, 64.25 (d,  $J_{P,C} = 6.2$  Hz), 103.73, 115.44, 120.10, 127.72 (d,  $J_{P,C} = 8.7$  Hz), 128.40 (d,  $J_{P,C} = 7.7$  Hz), 130.72, 140.89 (d,  $J_{P,C} = 2.9$  Hz), 149.74 (d,  $J_{P,C} = 1.8$  Hz), 158.89, 168.18;  $^{31}\text{P}\{^1\text{H}\}$  NMR (161.9 MHz, DMSO-*d*<sub>6</sub>, 30 °C)  $\delta = -4.78$ ; MS: (LSI) (M+H)<sup>+</sup> 369; HRMS: *m/z* Calcd for C<sub>16</sub>H<sub>22</sub>N<sub>2</sub>O<sub>6</sub>P (M+H)<sup>+</sup>: 369.12179 Found 369.12155; E.A. [Found C, 51.81; H, 5.71; N, 7.53; C<sub>16</sub>H<sub>21</sub>N<sub>2</sub>O<sub>6</sub>P requires C, 52.17; H, 5.75; N, 7.61%].

**3e** (THF) 1.349 g (3.55 mmol, 71%); mp = 245 °C (THF);  $^1\text{H}$  NMR (400.13 MHz, DMSO-*d*<sub>6</sub>, 30 °C)  $\delta = 0.92$  (s, 3H, CH<sub>3</sub>), 1.23 (s, 3H, CH<sub>3</sub>), 2.11 (s, 3H, CH<sub>3</sub>), 2.66 (s, 3H, CH<sub>3</sub>), 4.05 (dd,  $J_{H,Hgem} = 10.7$  Hz,  $J_{P,H} = 23.5$  Hz, 2Ha, CH<sub>2</sub>), 4.90 (d,  $J_{H,Hgem} = 10.4$  Hz, 2He, CH<sub>2</sub>), 7.35 (d,  $J_{H,H} = 8.5$  Hz, 1H, quin-H), 7.59 (s, 1H, quin-H), 8.34 (d,  $J_{H,H} = 8.5$  Hz, 1H, quin-H), 9.77 (s, 1H, OH), 10.62 (s, 1H, NH);  $^{13}\text{C}\{^1\text{H}\}$  NMR (100.4 MHz, DMSO-*d*<sub>6</sub>, 30 °C)  $\delta = 19.19, 20.95, 23.95, 24.81, 31.73$  (d,  $J_{P,C} = 6.0$  Hz), 78.26 (d,  $J_{P,C} = 6.9$  Hz), 103.46, 115.40, 120.23, 126.77 (d,  $J_{P,C} = 7.4$  Hz), 130.70 (d,  $J_{P,C} = 3.4$  Hz), 131.02, 140.65 (d,  $J_{P,C} = 3.4$  Hz), 150.09 (d,  $J_{P,C} = 1.7$  Hz), 159.14, 168.12;  $^{31}\text{P}\{^1\text{H}\}$  NMR (161.9 MHz, DMSO-*d*<sub>6</sub>, 30 °C)  $\delta = -11.61$ ;  $^{31}\text{P}$  NMR (161.9 MHz, DMSO-*d*<sub>6</sub>, 30 °C)  $\delta = -11.61$  (t,  $J_{P,H} = 23.4$  Hz); MS: (LSI) (M+H)<sup>+</sup> 381; HRMS: *m/z* Calcd for C<sub>17</sub>H<sub>22</sub>N<sub>2</sub>O<sub>6</sub>P (M+H)<sup>+</sup>: 381.12155 Found 381.12069, E.A. [Found C, 53.84; H, 5.63; N, 7.28; C<sub>17</sub>H<sub>21</sub>N<sub>2</sub>O<sub>6</sub>P requires C, 53.69; H, 5.57; N, 7.37%].

**3f** (MeOH) 1.014 g (3.40 mmol, 68%); mp = 226 °C (MeOH);  $^1\text{H}$  NMR (400.13 MHz, DMSO-*d*<sub>6</sub>, 30 °C)  $\delta = 2.68$  (s, 3H, CH<sub>3</sub>), 3.52 (d,  $J_{P,H} = 11.1$  Hz, 6H, CH<sub>3</sub>), 6.64 (s, 1H, quin-H), 7.15 (d,  $J_{H,H} = 8.2$  Hz, 1H, quin-H), 8.57 (d,  $J_{H,H} = 8.2$  Hz, 1H, quin-H), 10.94 (s, 1H, OH);  $^{13}\text{C}\{^1\text{H}\}$  NMR (100.4 MHz, DMSO-*d*<sub>6</sub>, 45 °C)  $\delta = 19.75, 52.68$  (d,  $J_{P,C} = 6.3$  Hz), 100.59, 112.85, 113.84, 117.54 (d,  $J_{P,C} = 7.7$  Hz), 132.73 (d,  $J_{P,C} = 2.1$  Hz), 138.50, 146.62 (d,  $J_{P,C} = 4.2$  Hz), 150.70, 153.68;  $^{31}\text{P}\{^1\text{H}\}$  NMR (161.9 MHz, DMSO-*d*<sub>6</sub>, 30 °C)  $\delta = -0.20$ ;  $^{31}\text{P}$  NMR (161.9 MHz, DMSO-*d*<sub>6</sub>, 30 °C)  $\delta = -0.20$  (q,  $J_{P,H} = 11.1$  Hz); MS: (LSI) (M+H)<sup>+</sup> 299; HRMS: *m/z* Calcd for C<sub>12</sub>H<sub>16</sub>N<sub>2</sub>O<sub>5</sub>P (M+H)<sup>+</sup>:

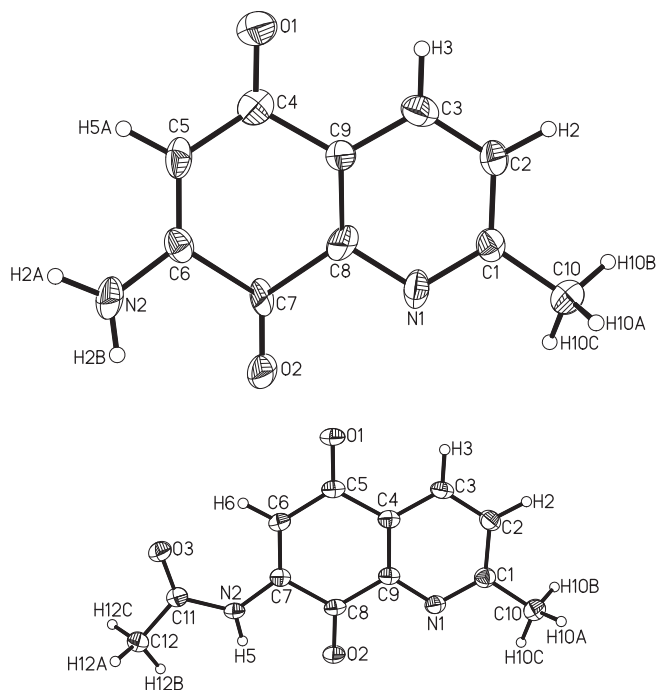


**Fig. 1.** Molecular structure diagrams of **2a** (upper) and **2b** (below). The thermal ellipsoids are drawn at the 50% probability level.

**Table 1**

Selected bond lengths for **2a**. Symmetry codes: (i)  $x + 1/2, -y + 3/2, z + 1/2$ ; (ii)  $-x + 3/2, y - 1/2, -z + 1/2$ .

	Exp.	Calc.		
<i>Bond lengths (Å)</i>				
C4–O1	1.233(2)	1.232	C14–O3	1.249(12)
C7–O2	1.213(19)	1.221	C17–O4	1.250(19)
C6–N2	1.341(2)	1.339	C16–N4	1.319(2)
<i>Hydrogen-bond geometry (Å, °)</i>				
D–H...A	D–H	H...A	D...A	D–H...A
O5–H5...O3	0.99(3)	1.81(3)	2.8018(19)	176.0(3)
N2–H2A...N3	0.88	2.30(1)	3.0468(19)	143.3(2)
N4–H4A...N1 <sup>i</sup>	0.88	2.15(6)	2.971(2)	155.2(3)
N4–H4A...O2 <sup>i</sup>	0.88	2.63(3)	3.274(2)	131.4(3)
N4–H4B...O5 <sup>ii</sup>	0.88	2.17(3)	2.9125(19)	142.3(4)

**Table 2**

Selected bond lengths for **2b**. Symmetry code: (i)  $-x + 4, -y + 1, -z + 1$ .

	Exp.	Calc.		Exp.	Calc.
<i>Bond lengths (Å)</i>					
C5–O1	1.222(2)	1.228	N2–C11	1.386(2)	1.388
C8–O2	1.214(2)	1.222	C11–O3	1.211(2)	1.218
C7–N2	1.378(2)	1.381			
<i>Hydrogen-bond geometry (Å, °)</i>					
D–H...A	D–H	H...A	D...A	D–H...A	
N2–H5...O2A	0.82(2)	2.23(2)	2.6360(18)	110.8(17)	
N2A–H5A...O2 <sup>i</sup>	0.82(2)	2.31(2)	3.1193(18)	167.7(19)	

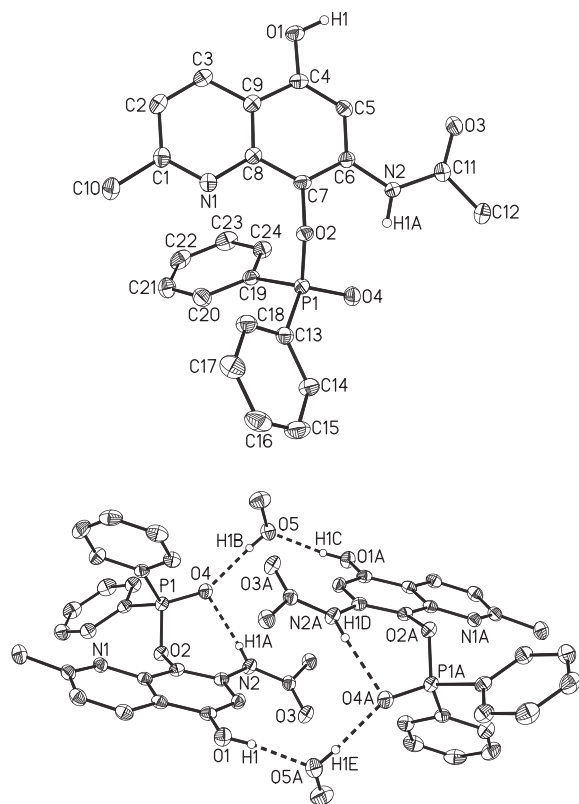


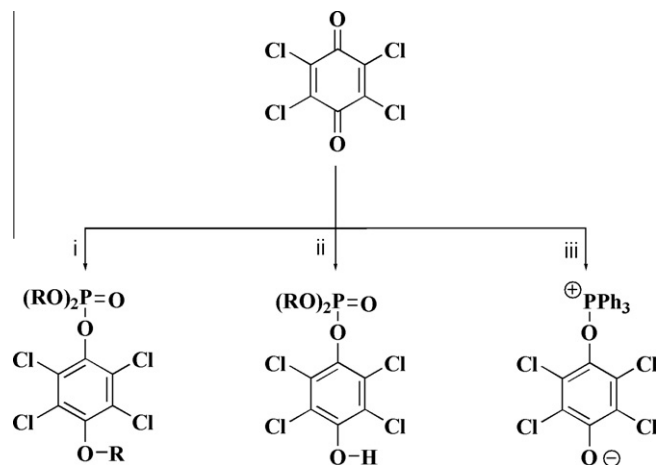
**Fig. 2.** Molecular structure of the ester **3a** (upper) and the interaction diagram between two molecules of **3a** and methanol (below). The thermal ellipsoids are drawn at 50% probability level. All hydrogen atoms other than H1, H1A and H1B have been omitted for clarity.

299.07968 Found 299.07964; E.A. [Found C, 48.19; H, 5.17; N, 9.27; C<sub>12</sub>H<sub>15</sub>N<sub>2</sub>O<sub>5</sub>P requires C, 48.33; H, 5.07; N, 9.39%].

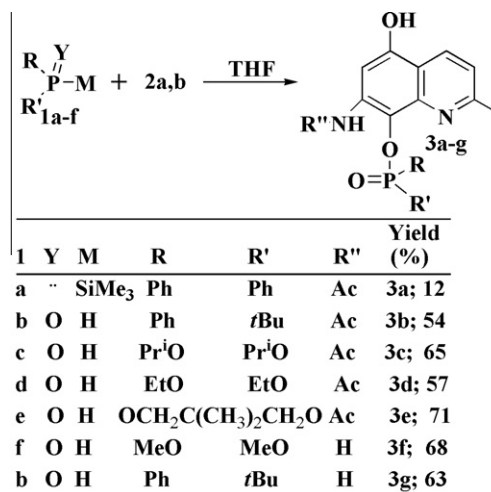
### 3. Results and discussion

Our present study describes electron transfer properties of the two structurally characterised compounds possesses quinoline-

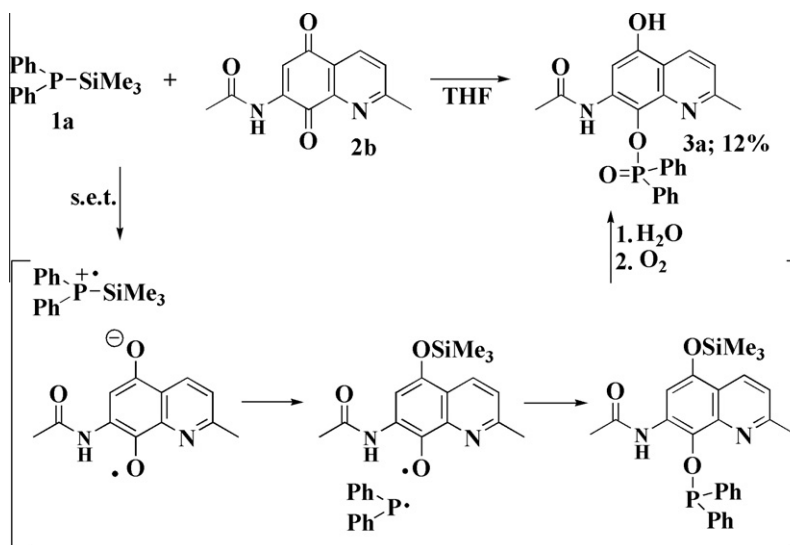
5,8-dione unit. The quinoline-5,8-dione derivatives 2-methyl-5,8-dioxo-5,8-dihydroquinoline-7-amine (**2a**) and N-(2-methyl-5,8-dioxo-5,8-dihydroquinolin-7-yl)acetamide (**2b**) were chosen as



**Scheme 2.** Reagents: (i) P(OR)<sub>3</sub>; (ii) (RO)<sub>2</sub>P(=O)H; (iii) PPh<sub>3</sub>.



**Scheme 3.** Synthesis of **3**.



**Scheme 1.** Reaction of **1a** with **2b**. Proposal of mechanism.

model compounds and characterised by crystal structure analysis (Fig. 1; Tables 1 and 2).

Compound **2a** crystallises with methanol in space group P21/n (No. 14), compound **2b** in P-1 (No. 2). The molecular ring systems are both essentially planar. The packing of the molecules **2a** and **2b** in the structure is stabilised by  $\pi$ - $\pi$  stacking interactions. Both compounds co-crystallised with CH<sub>3</sub>OH which is associated through strong C–O–H...O(C) hydrogen bonds. The molecules of **2a** are linked by weak bifurcated N2–H2A...N3, N1–H4AA...N4A and O5–H5...O3 hydrogen bonds, the molecules of **2b** by strong N2–H2B...O2A(C) and N2A–H2AB–O2(C) hydrogen bonds.

Compared to **2a**, the C5–C8 distances are longer in **2b** which could be explained by the resonance structures in **2a** which can

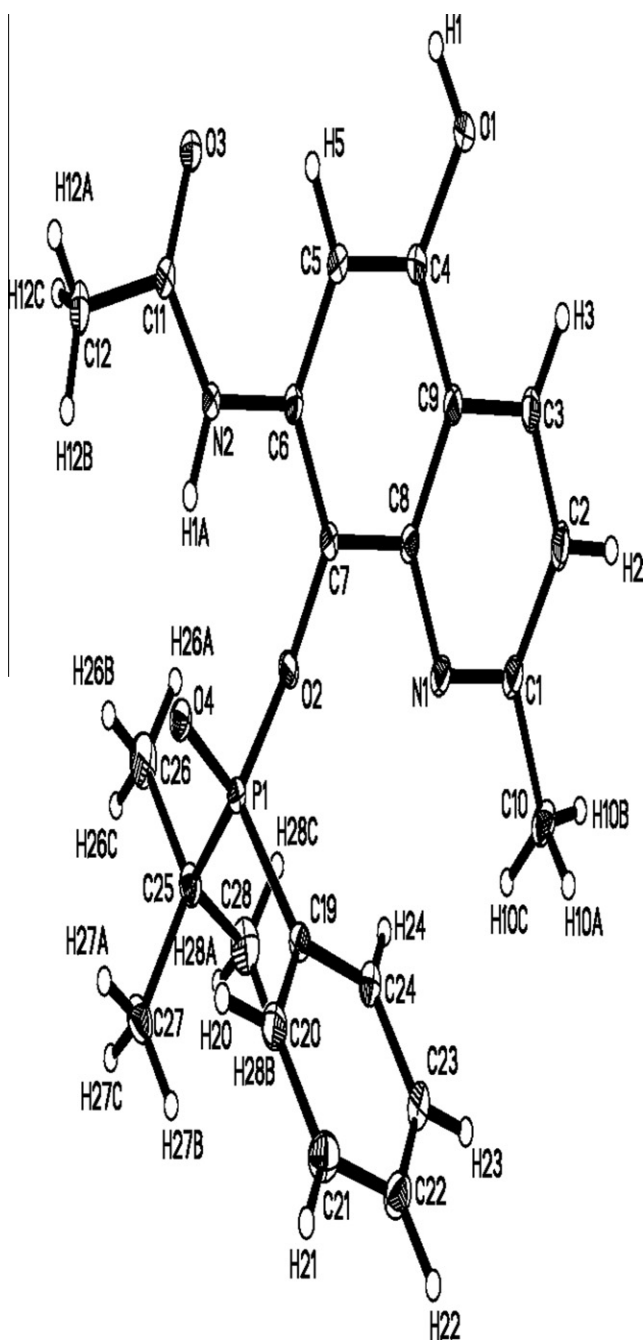


**Fig. 3.** Molecular structure diagram of **3b**. The thermal ellipsoids are drawn at the 50% probability level, for the sake of clarity, hydrogen atoms not involved in hydrogen bonds were omitted.

also explain the differences between the C=O distances [C7–O2 1.173(12) Å and C4–O1 1.210(12) Å].

The phosphorylation of lavendomycin and its structural building blocks is still not fully explored. To increase accessibility, the reaction between neutral silyl derivative of phosphorus nucleophile, i.e. Ph<sub>2</sub>P–SiMe<sub>3</sub> (**1a**) and **2b** was chosen. The reaction between neutral silyl derivatives of phosphorus nucleophiles are convenient reagents for creating C–P bonds during addition into carbonyl compounds [17,18]. In constitution of **2b** there are three possible centres of attack in the quinolidione ring: (a) the carbonyl carbon atoms (b) the carbonyl oxygen atoms, and (c) the activated carbon–carbon double bond. Additionally, there are two centres in its acyl group (a) the carbonyl carbon atom, and (b) the carbonyl oxygen atoms.

The reaction of **1a** with **2b** gave a complex reaction mixture. Among the products we isolated and structurally characterised the radical addition product **3a**, i.e. compound with the construction P–O–C. To the best of our knowledge this is the first example of the radical addition of silylated phosphane to carbonyl compound (Fig. 2).

Compound **3a** crystallises in space group P $\bar{1}$  (No. 2). The quinoline rings are practically planar. The packing of molecules in the structure is stabilised by N–H1A...O4(P) hydrogen bonds. The compound co-crystallised with CH<sub>3</sub>OH in a dimer form which is bound by (P)O4...H1B–O5, (C)O1–H1...O5A and N2–H1A–O4 hydrogen bonds.

A possible explanation of the formation of final product **3a** is a transfer of electron (SET) from the nucleophile **1a** to **2b** followed by the migration of the silyl group from cation radical of **1a** to the oxygen atom of anion radical of **2b**, giving the O- and P-centered radicals (Scheme 1). Next, phosphinyl and oxygen radicals react followed by oxygenation to **3a**. Possibly, the process occurs without formation of completely free radical intermediates, because tetraphenyldiphosphane was not detected in the reaction mixture, using <sup>31</sup>P NMR techniques. The redox addition approach presented here provides a direct route to a new class of compounds which are potentially useful from a biological, synthetic and coordination point of view.

However the reaction of quinones with tertiary phosphanes and phosphites is well reported in the literature and provide to variety of interesting products [19–24]. Ramirez et al. [19,20,22–25] reported the reaction of chloranil with a range of phosphorus compounds including trialkyl phosphites, dialkyl phosphates and triphenylphosphane to give transient red solutions from which the

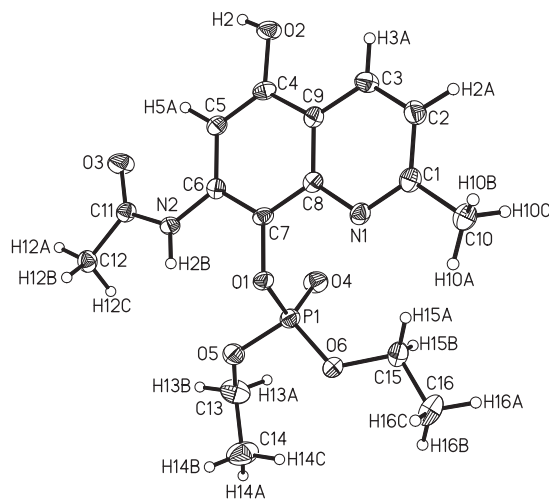


**Fig. 4.** Molecular structure diagram of **3d**. All hydrogen atoms other than H2 and H2B have been omitted for clarity. The thermal ellipsoids are drawn at the 50% probability level.

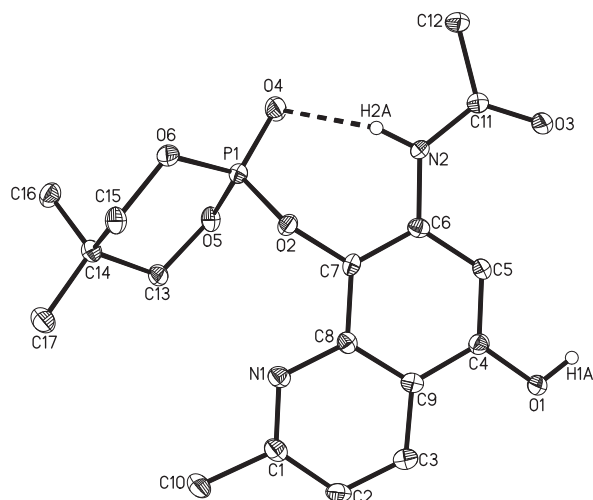


**Fig. 5.** Molecular structure of the ester **3e**. The thermal ellipsoids are drawn at 50% probability level. All hydrogen atoms other than H1A, H2A, H1AA and H2AA have been omitted for clarity.

quasi-phosphonium salt is obtained in the case of a phosphane, and the corresponding alkylated quinol phosphates in the case of alkyl phosphites, and hydroxyarylalkylphosphates in the case of dialkyl phosphates. They reported no chlorinated substitution products (Scheme 2).

The mechanism of these reactions have been investigated in some details, and the transient red colour attributed to free radicals intermediates detected by the EPR spectrum. Lucken [21] has shown that the spectrum is typical of that of a semiquinone. This may be formed of a charge-transfer complex. The

phenomenon would account for the appearance of deep-red colour in the solution.

Due to reactive phosphorus–hydrogen bonds the secondary phosphanes, their oxides and dialkyl (diaryl) phosphates are widely used reagents and synthetic intermediates [25–27]. Acid-catalyzed addition reactions into the carbonyl are presumed to proceed by nucleophilic attack of the phosphorus atom at the substrate which was previously activated by the acid, followed by subsequent deprotonation. This type of catalysis occurs because the conjugate acid of the carbonyl compound is much more electrophilic than the neutral molecule. To compare the reactivity of various three-coordinate phosphorus nucleophiles towards **2a** and **2b** a reaction between **1b** with **2b** and **2a** was performed. **1b** was used in the reaction with **2a** and **2b** in excess. The transformation leads to **3b** and **3g**, respectively with high yield (Scheme 3). The secondary phosphanes and their oxides demonstrate higher nucleophilicity than dialkyl phosphates or analogue compounds, which possess alkoxy or aryloxy substituents at the phosphorus atom. Because of this, commercially available dialkyl phosphates **1c**, **1d**, **1e** and **1f** were used in the reaction with **2a** and **2b** in excess. The conversion was unambiguous and gave a radical addition products **3c**, **3d**, **3e** and **3f** with high yield (Scheme 3; Figs. 3–6).

**3b** crystallises in space group P21/c (No. 14). The quinoline rings are practically planar. The packing of molecules in the structure is stabilised by  $\pi$ – $\pi$  stacking interactions and by O1–H1···O3, N2–H1A···O4 and C10–H10B···O3 hydrogen bonds.

**3d** crystallises in space group P-1 (No. 12). The quinoline rings are practically planar. The packing of molecules in the structure is stabilised by O2–H2···O3, N2–H2B···O1 and N2–H2B···O5 hydrogen bonds.

**3e** crystallises in space group P2(1)/c (No. 14). The quinoline rings is practically planar. The molecular structure is stabilized by an intramolecular N–H···O hydrogen bond. In addition, the

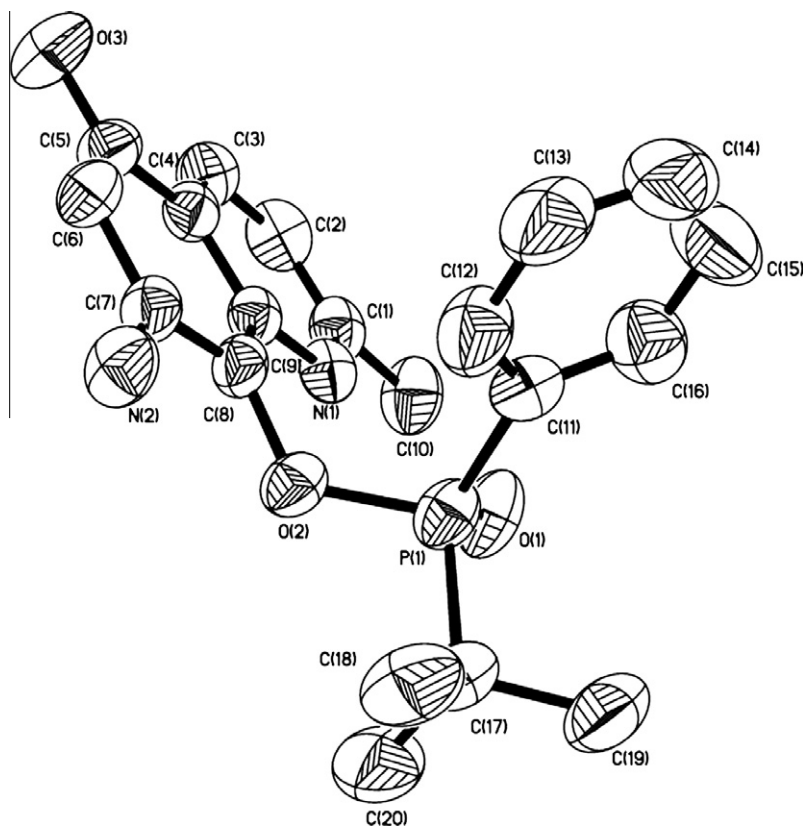


**Fig. 6.** Molecular structure of the **3g**. The thermal ellipsoids are drawn at 50% probability level.

molecules are linked by intermolecular O–H...O hydrogen bonds, the symmetry code is  $-x, 1-y, 1-z$ .

**3g** crystallises in space group P2(1)/c (No. 14). The quinoline rings is practically planar. The packing of molecules in the structure is stabilised by  $\pi$ – $\pi$  stacking interactions and by an intramolecular N–H...O hydrogen bond. In addition, the molecules are linked by intermolecular C–H...O hydrogen bonds, the symmetry code is  $-x, 1-y, 1-z$ .

The neutral phosphorus nucleophiles **1a**, **1b**, **1c**, **1d**, **1e** and **1f** allowed the radical addition to **2a** and **2b** giving exclusively O(2)-phosphorylated products **3a**, **3b**, **3c**, **3d**, **3e**, **3f** and **3g**, respectively, with high yield. The smaller yield of **3a** could be explained by hydrolysis during isolation (chromatography). On the  $^{31}\text{P}$  NMR spectra of the reaction mixtures, in all cases no signal from products with a P–P bond, such as the diphosphanes, diphosphane dioxides or hypophosphoric acid esters was detected. Presented here radical addition reaction is chemoselective. We do not isolated reversed products, i.e. O1(C4)-phosphorylation, and addition products into acyl group, or into the activated carbon–carbon double bond (Michael type products). All results support presents a charge-transfer complex, rather than free radicals.

### 3.1. Cyclic voltammetry

Described here the redox properties of **2a** and **2b** provided opportunities for advancing electroanalytical measurements. The cyclic voltammetry studies show similar redox properties for both **2a** and **2b** (Fig. 7). They undergo reversible one-electron reductions at  $-1.06$  V (vs. Fc/Fc $^+$ ) (**2b**) and  $-1.20$  V (vs. Fc/Fc $^+$ ) (**2a**). The second reduction at  $-1.66$  V is nearly reversible only for **2b**. The second reduction for **2a** at around  $-1.79$  V (vs. Fc/Fc $^+$ ) is irreversible at 25 °C, at lower temperature ( $-60$  °C) it becomes more reversible. The first reduction potential of **2a** is shifted to a more negative value in comparison with that of **2b** which suggests that this precursor is a poorer electron acceptor and that the electron-withdrawing acyl group makes **2b** a better electron acceptor.

The first reduction potential corresponds with the electrochemical behaviour of natural occurring quinones [1–3,28]. In a broader sense it also highlights the possible role of electron transfer in the biological activity of naturally occurring quinolinediones such as lavendamycin [8].

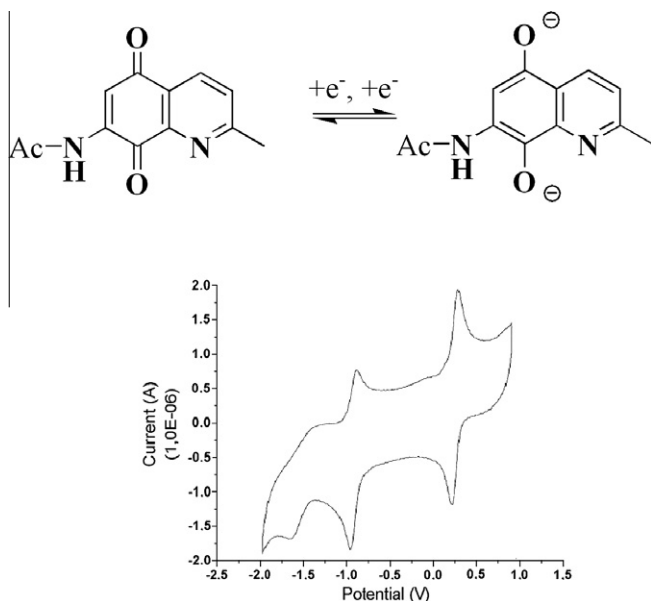


**Fig. 7.** Cyclic voltammetry of **2b** in  $\text{CH}_2\text{Cl}_2$  (0.1 M  $n\text{-Bu}_4\text{NBF}_4$  as electrolyte; Ag/Ag $^+$  reference electrode, 20 °C, Fc/Fc $^+$  (right) as internal standard).

**Table 3**

Selected bond lengths and angles for **3a**. Symmetry code: (i)  $-x+2, -y, -z+1$ .

Exp.		Calc.		Exp.		Calc.	
<i>Bond lengths (Å)</i>							
P1–O4	1.492(14)	1.504	N2–C11	1.362(2)	1.367		
P1–O2	1.598(13)	1.636	C4–C5	1.374(3)	1.375		
O1–C4	1.359(2)	1.366	C5–C6	1.416(3)	1.422		
O2–C7	1.404(2)	1.391	C6–C7	1.372(3)	1.396		
O3–C11	1.222(2)	1.225	C8–C9	1.418(3)	1.429		
N2–C6	1.414(2)	1.398					
<i>Bond angles (°)</i>							
Exp.		Calc.		Exp.		Calc.	
C6–C7–O2	120.41(16)	121.42	O2–P1–O4	110.86(8)	113.72		
C6–N2–C11	127.44(17)	128.64	N2–C11–O3	123.26(18)	124.80		
C7–O2–P1	124.09(11)	128.88	C5–C4–O1	122.59(17)	122.40		
<i>Hydrogen-bond geometry (Å, °)</i>							
D–H...A	D–H	H...A	D...A	D–H...A			
O1–H1...O5A <sup>i</sup>	0.89(3)	1.78(3)	2.670(2)	175(3)			
N2–H1A...O4	0.86(2)	2.13(3)	2.964(2)	163(2)			
O5–H1B...O4	0.80(3)	1.95(3)	2.735(2)	171(3)			

### 3.2. DFT calculations

In order to get further insight into the electronic structures and bonding properties of the compounds, the DFT calculations were carried out. First the geometries of the compounds were optimized in singlet states using the DFT method with a B3LYP functional and next the electronic structures of the compounds were calculated. In general, the predicted bond lengths and angles are in a very good agreement with the values based on the X-ray crystal structure data, and the general trends observed in the experimental data are well reproduced in the calculations as can be seen in Tables 1–7. Among the studied compounds in the first group belong quinone **2a** and **2b**. The natural atomic charges on the heteroatoms of these compounds are taken from the Natural Population Analysis and are close to each other; **2a**: N(quinoline)  $-0.42$ , N(amine)  $-0.79$ , O(1)  $-0.58$ , O(2)  $-0.51$ ; **2b**: N(quinoline)  $-0.42$ ; N(amide)  $-0.63$ , O(1)  $-0.53$ , O(2)  $-0.52$ . The atomic charge calculations can give a feature for the relocation of the electron density of the compounds, but the local concentration and local depletion of electron charge density allow us to determine whether the nucleophile or electrophile can be attracted. Since the electron distribution is not apparent from the partial atomic charges, Fig. 8 shows the plots of the electrostatic potentials for the compounds. The isoelectronic contours are plotted at 0.05 a.u. (31 kcal/mol). The colour code of

**Table 4**

Selected bond lengths and angles for **3b**. Symmetry code: (i)  $-x, -y+1, -z$ ; (ii)  $-x, -y+2, -z$ .

Exp.		Calc.		Exp.		Calc.	
<i>Bond lengths (Å)</i>							
P1–O4	1.487(6)	1.508	C11–C12	1.499(13)	1.521		
P1–O2	1.604(6)	1.638	C4–C5	1.370(12)	1.375		
O1–C4	1.357(10)	1.366	C5–C6	1.417(12)	1.422		
O2–C7	1.399(10)	1.392	C6–C7	1.379(12)	1.398		
O3–C11	1.236(11)	1.225	C7–C8	1.423(11)	1.422		
N2–C6	1.418(11)	1.400	C8–C9	1.415(12)	1.429		
N2–C11	1.351(11)	1.381	C1–C10	1.500(13)	1.510		
<i>Bond angles (°)</i>							
Exp.		Calc.		Exp.		Calc.	
O4–P1–O2	113.47(3)	113.14	C6–C7–O2	121.83(7)	121.99		
C7–O2–P1	126.92(5)	130.17	O1–C4–C5	123.44(8)	122.44		
<i>Hydrogen-bond geometry (Å, °)</i>							
D–H...A	D–H	H...A	D...A	D–H...A			
O1–H1...O3 <sup>i</sup>	0.853(14)	1.818(14)	2.6692(10)	175.2(13)			
N2–H1A...O4	0.890(12)	1.897(12)	2.7512(10)	160.3(11)			
C10–H10B...O3 <sup>ii</sup>	0.936(14)	2.471(14)	3.3928(12)	168.4(11)			

**Table 5**

Selected bond lengths and angles for **3d**. Symmetry code: (i)  $-x + 1, -y - 1, -z + 1$ ; (ii)  $-x, -y, -z + 1$ .

	Exp.	Calc.		Exp.	Calc.
<i>Bond lengths (Å)</i>					
P1–O4	1.460(2)	1.478	C11–C12	1.496(4)	1.522
P1–O1	1.556(2)	1.624	C4–C5	1.377(4)	1.378
O2–C4	1.354(3)	1.365	C5–C6	1.415(4)	1.418
O1–C7	1.404(3)	1.394	C6–C7	1.372(4)	1.389
O3–C11	1.230(3)	1.223	C7–C8	1.414(4)	1.417
N2–C6	1.424(3)	1.402	C8–C9	1.415(4)	1.427
N2–C11	1.353(3)	1.378	C1–C10	1.502(4)	1.510
<i>Bond angles (°)</i>					
	Exp.	Calc.		Exp.	Calc.
O4–P1–O1	114.24(11)	117.63	C6–C7–O1	119.80(2)	118.66
C7–O1–P1	118.97(16)	119.54	O2–C4–C5	116.20(2)	116.42
<i>Hydrogen-bond geometry (Å, °)</i>					
D–H...A	D–H	H...A	D...A	D–H...A	
O2–H2...O3 <sup>i</sup>	0.84(4)	1.81(4)	2.643(3)	174.0(4)	
N2–H2B...O1 <sup>ii</sup>	0.88	2.35(4)	3.090(3)	142.3(4)	
N2–H2B...O5	0.88	2.56(3)	3.255(3)	136.5(4)	

**Table 6**

Selected bond lengths and angles for **3e**. Symmetry code: (i)  $-x, 1 - y, 1 - z$ .

	Exp.	Calc.		Exp.	Calc.
<i>Bond lengths (Å)</i>					
P1–O4	1.461(3)	1.480	N2–C11	1.349(4)	1.383
P1–O2	1.581(2)	1.597	C4–C5	1.371(5)	1.374
O1–C4	1.360(4)	1.365	C5–C6	1.411(5)	1.421
O2–C7	1.402(4)	1.399	C6–C7	1.393(4)	1.397
O3–C11	1.221(4)	1.224	C8–C9	1.421(5)	1.429
N2–C6	1.407(4)	1.398			
<i>Bond angles (°)</i>					
C6–C7–O2	120.40(3)	121.33	O2–P1–O4	113.77(3)	113.96
C6–N2–C11	129.20(3)	128.49	N2–C11–O3	123.80(3)	124.79
C7–O2–P1	127.60(2)	127.49	C5–C4–O1	122.80(3)	122.48
<i>Hydrogen-bond geometry (Å, °)</i>					
D–H...A	D–H	H...A	D...A	D–H...A	
O1–H1A...O5 <sup>i</sup>	0.84(3)	1.83(3)	2.670(3)	178.7(3)	
N2–H2A...O4	0.88(2)	2.07(3)	2.846(4)	146.0(2)	

**Table 7**

Selected bond lengths and angles for **3g**. Symmetry code: (i)  $-1 - x, 1 - y, 1 - z$ .

	Exp.	Calc.		Exp.	Calc.
<i>Bond lengths (Å)</i>					
P1–O1	1.485(4)	1.4925	N1–C1	1.341(7)	1.3210
P1–O2	1.618(4)	1.6570	N2–C7	1.351(7)	1.3947
P1–C11	1.783(7)	1.8230	N1–C9	1.378(7)	1.3572
P1–C17	1.810(6)	1.8690	O3–C5	1.342(7)	1.3681
O2–C8	1.404(7)	1.3871			
<i>Bond angles (°)</i>					
O1–P1–C11	111.5(3)	113.93	O1–P1–O2	111.8(2)	119.13
O2–P1–C11	106.0(3)	105.44	O2–P1–C17	102.0(3)	97.80
O1–P1–C17	112.5(3)	110.34	C11–P1–C17	112.5(3)	108.74
<i>Hydrogen-bond geometry (Å, °)</i>					
D–H...A	D–H	H...A	D...A	D–H...A	
C3–H3A...O3 <sup>i</sup>	0.93	2.55	3.344(8)	143.8	
N2–H2A...O2	0.857(19)	2.41(5)	2.713(6)	102(3)	

these maps is in the range of 0.05 a.u. (deepest red) to  $-0.005$  a.u. (deepest blue), where blue indicates the strongest attraction and red indicates the strongest repulsion. Regions of negative  $V(r)$  are usually associated with the lone pairs of electronegative atoms. The negative potential in the studied compounds wraps the oxygen atoms and as one can see in the Fig. 8, negative potentials on oxygen atoms in position 8 of quinoline ring are smaller than the ones on positions 5. The calculated values could explain the preferred selectivity of phosphorylation.

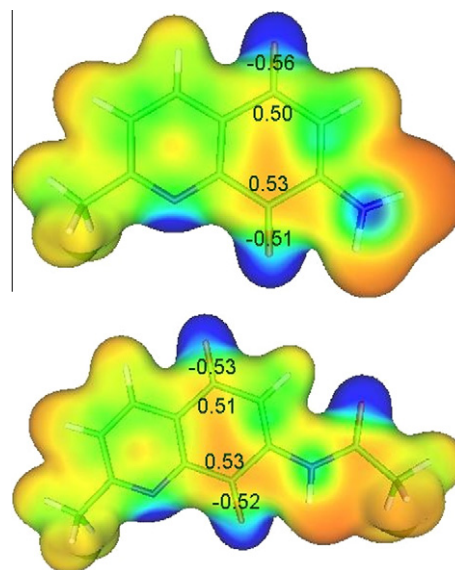


**Fig. 8.** Electrostatic potential (ESP) surfaces of **2a** (upper) and **2b** (below). ESP surface is shown both in space (with positive and negative regions shown in blue and red, respectively) and mapped on electron densities (in the range of 0.05 a.u. – deepest red-to-0.005 a.u. – deepest blue) of the molecule (ESP colour scale is such that  $\delta^+ \rightarrow \delta^-$  in the direction red  $\rightarrow$  blue). (For interpretation of the references to colour in this figure legend, the reader is referred to the web version of this article.)

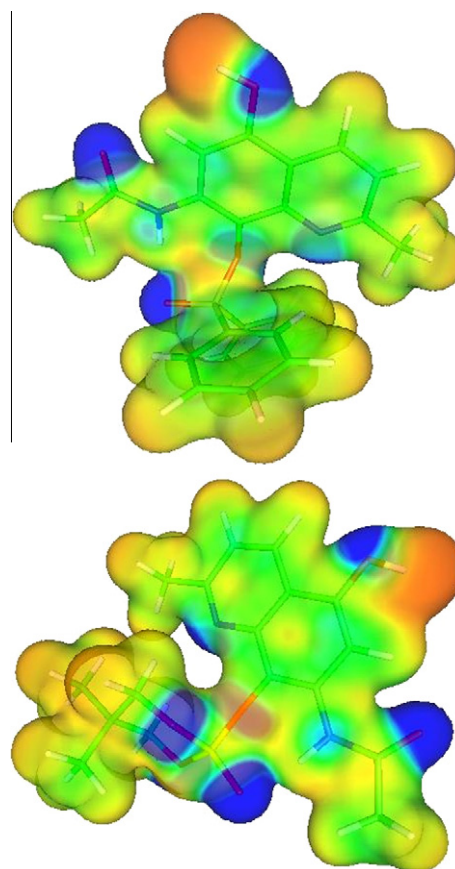


**Fig. 9.** Electrostatic potential (ESP) surfaces of **3a** (upper) and **3e** (below).

The natural phosphorus charges on the phosphate derivatives are about 2.3 in the phenyl phosphinate **3a**, **3b**, **3g** and about 2.6 in the case of **3d**, **3e** phosphate. The EPS surfaces of **3a** and **3e** are depicted on the Fig. 9 with the same parameters as on Fig. 8.

The energy of highest occupied and lowest virtual molecular orbitals of quinone type compounds are negative and close to:  $-6.28$ ,  $-6.83$  eV (HOMO) and:  $-2.84$ ,  $-3.17$  eV (LUMO) for **2a**, **2b**, respectively. In the case of phosphinate and phosphate derivatives the HOMO–LUMO gaps (**3a**, **3b**, **3e**, **3g**:  $\sim 4.16$  eV; **3d**:  $4.27$  eV) are bigger, though the energy levels are less negative which suggest strong acceptor affinity of these compounds. The partial density of states (PDOS) in terms of Mulliken population analysis were calculated using the GaussSum program which provides a pictorial representation of MOs compositions. The compounds were divided in quinoline and phosphate fragments. Fig. 10 represents the PDOS diagrams.

As can be seen the HOMO orbitals are mainly localised on the quinoline fragments and the phosphate fragment plays a role in lowering the HOMO and LUMO orbitals. In the case of compounds **3a**, **3b** containing phenyl phosphinate moiety with  $\pi$ -acceptor properties, which is connected to the lower LUMO orbitals, and are stronger compared with the phosphate derivatives. To estimate bonds between phosphinate/phosphate and quinoline fragments in the compounds the Mayer bonds orders were calculated and have values  $1.78$  (**3a**),  $1.75$  (**3b**, **3g**),  $1.98$  (**3d**) and  $1.90$  (**3e**). As can be seen from the bond orders, the **3d** compound should be more stable in terms of P–O(quin) bond break. At the next step the energy decomposition analyses of the studied compounds based on the work of Morokuma [29] and the extended transition state (ETS) partitioning scheme of Ziegler [30] have been carried out using ADF program at the level of B3LYP/DZP. The binding energies of the compounds were calculated as the difference between the energy of whole molecule with the optimized geometry and the energies of the optimized fragments phosphinate or phosphate chain and quinoline parts, respectively. The calculations were carried

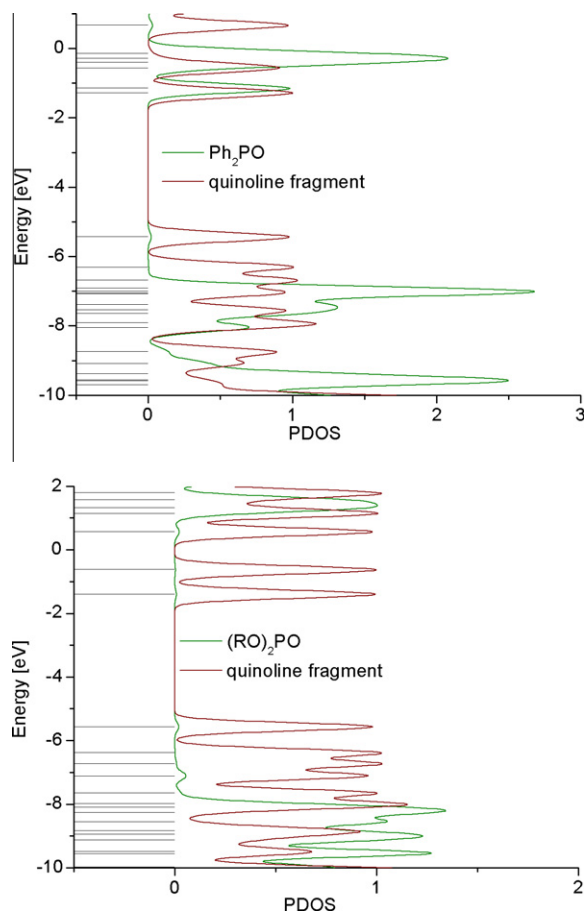


Fig. 10. Partial density of states of **3a** (upper) and **3e** (below).

out in methanol solvent as more realistic than the calculation in gas phase. The obtained energies:  $-212.58$  (**3a**),  $-208.71$  (**3b**),  $208.29$  (**3g**) and  $-230.96$  (**3d**),  $-235.11$  (**3e**) kcal/mol indicated that the phosphate derivatives are more stable.

#### 4. Conclusion

This study describes electron transfer properties of the structurally characterised compounds **2a** and **2b**. All employed neutral phosphorus nucleophiles **1b–f** and the silylphosphine **1a** reacted in a similar fashion with the quinone **2a** and **2b** to produce the corresponding addition products **3a**, **3b**, **3c**, **3d**, **3e**, **3f** and **3g** which were characterised by spectroscopic and analytical techniques. Furthermore, neither free radical intermediates nor the radical coupling product with a P–P bond, such as the diphosphanes, diphosphane dioxides or hypophosphoric acid esters was detected in these reactions, which strongly suggests that the process occurs without the formation of completely free radical species. The cyclic voltammetry measurements showed similar redox properties for both **2a** and **2b**. The first reduction potential corresponds with the electrochemical behaviour of natural occurring quinones. The calculated values could explain the preferred selectivity of phosphorylation.

#### 5. Supplementary material

CCDC – 726156 (for **2a**), 726157 (for **2b**), 726158 (for **3a**), 734355 (for **3b**), 760552 (for **3d**), 767288 (for **3e**) and 782763 (for **3g**) contains the supplementary crystallographic data for this paper. These data can be obtained free of charge from <http://www.ccdc.cam.ac.uk/conts/retrieving.html>, or from the Cambridge Crystallographic Data Centre, 12 Union Road, Cambridge CB2 1EZ, UK; fax: +44 1223 336 033; or e-mail: [deposit@ccdc.cam.ac.uk](mailto:deposit@ccdc.cam.ac.uk) Calculations have been carried out in Wroclaw Centre for Networking and Supercomputing (<http://www.wcss.wroc.pl>).

#### Acknowledgments

We thank the DAAD for the award of a fellowship to J.E. Nycz. This study was supported by Polish Ministry of Science No. NN405178735. Calculations have been carried out in Wroclaw Centre for Networking and Supercomputing (<http://www.wcss.wroc.pl>).

#### References

- [1] P.A. Frey, *Chem. Rev.* 90 (1990) 1343–1357.
- [2] S.E. Wolkenberg, D.L. Boger, *Chem. Rev.* 102 (2002) 2477–2495.
- [3] H. Ishikita, E.W. Knapp, *J. Biol. Chem.* 278 (2003) 52002–52011.
- [4] T.W. Doyle, D.M. Balitz, R.E. Grulich, D.E. Net, S.J. Gould, C. Tann, A.E. Moews, *Tetrahedron Lett.* 22 (1981) 4595–4598.
- [5] M. Shibata, M. Uyeda, Y. Kido, N. Toya, R. Nakashima, R. Terazumi, *J. Antibiot.* 33 (1980) 1231–1235.
- [6] D.M. Balitz, J.A. Bush, W.T. Bradner, T.W. Doyle, F.A. O'Herron, D.E. Nettleton, *J. Antibiot.* 35 (1982) 259–264.
- [7] D.L. Boger, M. Yasuda, L.A. Mitscher, S.D. Drake, P.A. Kitos, S.C. Thompson, *J. Med. Chem.* 30 (1987) 1918–1928.
- [8] R. Wolfenden, Y.-L. Liang, M. Matthews, R. Williams, *J. Am. Chem. Soc.* 109 (1987) 463–466.
- [9] J.E. Nycz, *Pol. J. Chem.* 83 (2009) 589–594.
- [10] J.E. Nycz, *Pol. J. Chem.* 83 (2009) 1637–1642.
- [11] M. Behforouz, W. Cai, M.G. Stocksdales, J.S. Lucas, J.Y. Jung, D. Briere, A. Wang, K.S. Katzen, N.C. Behforouz, *J. Med. Chem.* 46 (2003) 5773–5780.
- [12] M. Behforouz, J. Haddad, W. Cai, M.B. Arnold, F. Mohammadi, A.C. Sousa, M.A. Horn, *J. Org. Chem.* 61 (1996) 6552–6555.
- [13] S.E. Tunney, J.K. Stille, *J. Org. Chem.* 52 (1987) 748–753.
- [14] G.M. Sheldrick, *SHELXTL-97*, University of Göttingen, 1997.
- [15] G.M. Sheldrick, *Acta Cryst. A* 64 (2008) 112–122.
- [16] L. Coudray, J.-L. Montchamp, *Eur. J. Org. Chem.* (2008) 3601–3613.
- [17] M. Hayashi, Y. Matsuura, Y. Watanabe, *Tetrahedron Lett.* 45 (2004) 9167–9169.

- [18] D. Enders, A. Saint-Dizier, M.-I. Lannou, A. Lenzen, *Eur. J. Org. Chem.* (2006) 29–49.
- [19] F. Ramirez, S. Dershowitz, *J. Am. Chem. Soc.* 81 (1959) 587–590.
- [20] F. Ramirez, E.H. Chen, S. Dershowitz, *J. Am. Chem. Soc.* 81 (1959) 4338–4342.
- [21] E.A.C. Lucken, *J. Chem. Soc.* (1963) 5123–5127.
- [22] F. Ramirez, S.B. Bhatia, A.V. Patwardhan, E.H. Chen, C.P. Smith, *J. Org. Chem.* 33 (1968) 20–24.
- [23] R.O. Duthaler, P.A. Lyle, C. Heuberger, *Helv. Chim. Acta* 67 (1984) 1406–1426.
- [24] F. Ramirez, S. Dershowitz, *J. Org. Chem. Soc.* 22 (1957) 1282–1283.
- [25] S. Burck, D. Gudat, M. Nieger, W.-W. du Mont, *J. Am. Chem. Soc.* 128 (2006) 3946–3955.
- [26] R.B. King, *J. Org. Chem.* 41 (1976) 972–977.
- [27] F. Wang, X. Liu, X. Cui, Y. Xiong, X. Zhoy, X. Feng, *Chem. Eur. J.* 15 (2009) 589–592.
- [28] J.E. Nycz, G. Malecki, M. Morag, G. Nowak, L. Ponikiewski, J. Kusz, A. Switlicka, *J. Mol. Struct.* 980 (2010) 13–17.
- [29] K.J. Morokuma, *Chem. Phys. Lett.* 9 (1971) 129–132.
- [30] T. Ziegler, A. Rauk, *Theor. Chim. Acta* 46 (1977) 1–10.